Rock Dynamics – Experiments, Theories and Applications – Li, Li & Zhang (Eds)
© 2018 Taylor & Francis Group, London, ISBN 978-0-8153-9667-3

Simulation of strong motions and surface rupture of the 2014 Northern Nagano Earthquake

N. Iwata, R. Kiyota, K. Adachi & Y. Takahashi
Chuden Engineering Consultants Co. Ltd., Hiroshima, Japan

Ö. Aydan
Department of Civil Engineering, University of the Ryukyus, Okinawa, Japan

F. Miura
Graduate School of Science and Engineering, Yamaguchi University, Yamaguchi, Japan

T. Ito
Institute of Fluid Science, Tohoku University, Sendai, Japan

ABSTRACT: As the 1999 Chi-chi earthquake and the 1999 Kocaeli earthquake damaged many important structures due to surface rupture as well as strong motions, displacement and inclination of ground surface have become the significant issues in engineering. Most analytical methods do not evaluate displacement and strong motions at the same time. In this study, the authors conducted fault rupture simulation using three dimensional finite element method (3D-FEM) for the 2014 Northern Nagano Earthquake caused by the Kamishiro Fault, and confirmed the applicability of numerical method and conditions, such as spring stiffness of joint elements, FEM mesh size of a fault plane and the constitutive relation during stress drop, by comparing results with the observed ground motions and displacement. The computational results confirmed that the displacement and strong motion can be evaluated simultaneously using appropriate constitutive parameters and fine FEM mesh with a size less than 150 m.

1 INTRODUCTION

The 1999 Chi-chi earthquake and the 1999 Kocaeli earthquake damaged many important structures due to surface rupture as well as high strong motions induced by the earthquake faults, which indicated the significance of displacement and inclination of ground surface on the response and damage of structures. Generally strong motions are estimated by Green's function method and fault displacement is estimated from geological surveys. However an earthquake occurs by rupture of earthquake source fault. When the displacement is large, it will reach the ground surface and appear as a surface rupture. Therefore, ideal analytical model should be able to simulate a fault rupture process and estimate displacement and strong motion at the same time. Fault rupture simulations by Finite Difference Method (FDM), Finite Element Method (FEM) and Boundary Element Method (BEM) are generally carried out. However, they have not become practical as analytical results greatly vary according to assumed initial stress conditions and modeling of fault rupture.

In the past study, Iwata et al. (2016) conducted fault rupture simulation using 3D-FEM for the 2014 Northern Nagano Earthquake induced by the Kamishiro Fault (M_w6.3), which is a thrust fault type earthquake with an observed surface rupture of 9km in length. The analytical method and modeling of fault is dynamic response analysis considering fault rupture process proposed by Toki & Miura (1985) and Toki & Sawada (1988). Although the surface displacement response was in good agreement with the actual displacement, the acceleration response was not well simulated due to FEM mesh size, constitutive relation of fault plane and so on.

In this study, we carried out a series of numerical analyses on fault rupture simulation under various conditions to investigate the influence of spring stiffness of joint element, variation of FEM mesh size of a fault plane and the constitutive relation during stress drop. Validity of parameters and modeling was evaluated by comparison with the observed surface ground motions recorded at K-NET Hakuba station located approximately 0.5km away from surface rupture on the footwall side of the fault.

2 OUTLINE OF ANALYTICAL METHOD

If the equation of motion involves the rupture movement of fault plane, it is necessary to treat the motion as a nonlinear problem. Therefore, it is appropriate to obtain a solution for the equation of motion not in frequency domain but rather in the time domain. The destruction process of dislocation and the dynamic behavior of ground are calculated by solving the equation of motion using stress drop of dislocation as external force. The equation of motion at time step n is written as;

$$[M]\{\ddot{u}\}_n + [C]\{\dot{u}\}_n + [K]\{u\}_n = \{F(n,s)\} \tag{1}$$

where $[M]$ is mass matrix, $[C]$ is damping matrix, $[K]$ is stiffness matrix, $\{\ddot{u}\}$ is acceleration vector, $\{\dot{u}\}$ is velocity, $\{u\}$ is displacement and $\{F(n,s)\}$ is the external force vector calculated from the dynamic stress drop; n and s stand for time step and nodal pairs where fault rupture takes place, respectively. The damping matrix $[C]$ is obtained from the linear combination of $[M]$ and $[K]$, which is called Rayleigh damping. Eq.(1) is solved using the Newmark's β method, $\beta = 0.25$, $\gamma = 0.5$, at each time interval. To solve the nonlinear equation of motion, we employed the load transfer method utilizing initial stiffness method (Toki & Miura, 1985 and Toki & Sawada, 1988).

The fault plane is modeled by joint elements shown in Figure 1. The shear spring K_s, K_r and normal spring K_n are connected between nodal points of solid elements and a sliding occurs according to Mohr-Coulomb failure criterion. The constitutive relation that represents the relation between the shear stress and deformation is shown in Figure 2. When the calculated shear stress τ is less than the peak stress τ_y, the stress-deformation relation is linear with the joint stiffness K_s, K_r.

Sliding takes place if the shear stress τ reaches the peak stress τ_y and stress drop occurs. The shear stress becomes equivalent the residual strength τ_r and stress drop $\Delta\tau_d$ (= τ_y - τ_r) is released and

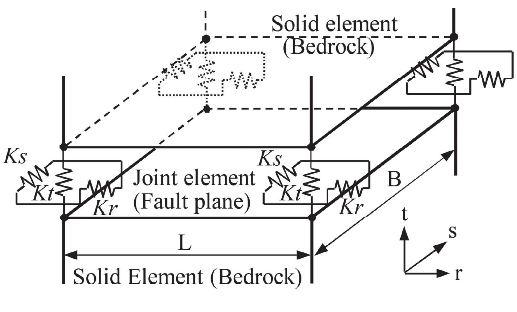

Figure 1. Schematic diagram of joint element in 3D-FEM.

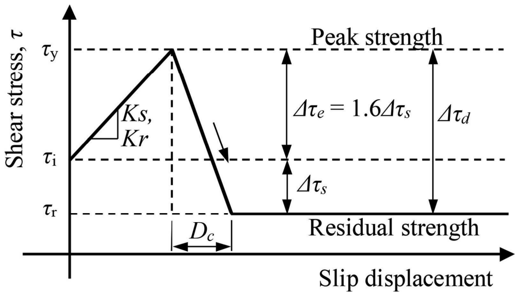

Figure 2. Constitutive relation of joint element.

spread to nearby elements. In this way, the released stress drop in the epicenter is triggered, shear failure spreads to surrounding areas with increasing of shear stress. In the past study, the peak stress instantly becomes equivalent to the residual strength, however, the peak stress in the slip-weakening behavior based on laboratory experiments exponentially decreases with the increase of relative displacement (Ohnaka & Yamashita, 1989). In this study, relationship between stress drop, $\Delta\tau_d$, and critical slip displacement, D_c, is assumed linear as shown in Figure 2.

3 OVERVIEW OF THE 2014 NORTHERN NAGANO EARTHQUAKE

The 2014 Northern Nagano Earthquake induced by the Kamishiro Fault, with a moment magnitude of 6.3, occurred at 22:08 JST on November 22 at northern part of Nagano Prefecture. Figure 3 shows schematic diagram of the fault plane. The fault plane is 15 km long and 12km wide and the focal depth are estimated to be 5–6 km (F-net, 2014; ERI, 2014; JMA, 2014). The slip sense is estimated thrust faulting with left-lateral strike slip in N16E-50E and rake angle of 50 degrees (F-net, 2014; ERI, 2014). The surface rupture appeared at southern 9km of the fault and the average dislocation in fault plane was 80cm.

Figure 4 shows acceleration records at K-NET Hakuba station, which is one of the strong motion stations of the dense strong motion network operated by NIED and located approximately 0.5km away from surface rupture in the west on the footwall side of the earthquake fault. The maximum accelerations was 570Gal horizontally and 278 Gal vertically. The displacement response calculated using the EPS method proposed by Aydan & Ohta (2011), which is an integration technique to obtain ground motions with the consideration of device operation features, fault rupture duration and arrival time difference of P-wave and S-wave.

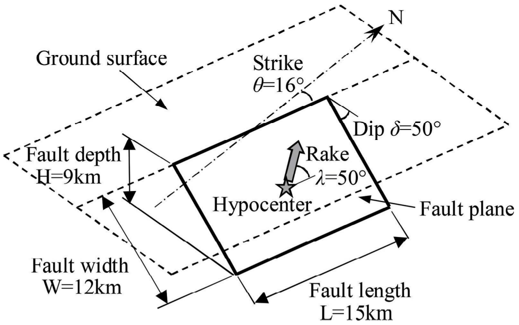

Figure 3. Schematic diagram of the fault plane.

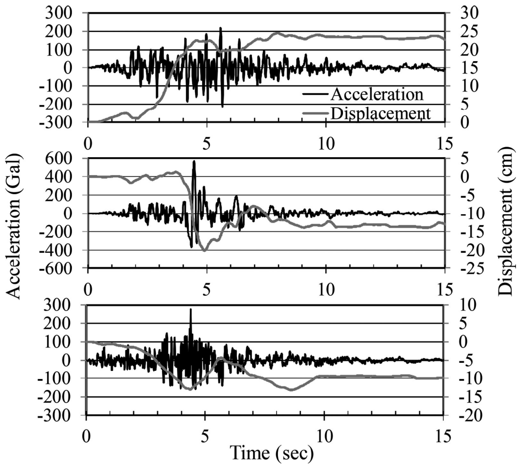

Figure 4. Acceleration records at K-NET Hakuba station and displacement time histories calculated by the EPS method.

From these results, residual displacement was obtained as 24 cm horizontally and 10 cm vertically at Hakuba site.

Figure 5 shows acceleration response spectrum at K-NET Hakuba station. The spectrum in N-S direction is larger than that in E-W direction for whole periods, and the predominant period in N-S and E-W direction are around 0.2–0.3 s, 0.1–0.3 s respectively and the predominant period in N-S direction is slightly larger than that in E-W direction. The predominant period in U-D direction is less than 0.1 s and shorter than that in horizontal direction.

4 ANALYTICAL CONDITIONS AND PARAMETERS

To investigate the influence of spring stiffness of joint element, the division size of FEM mesh of a fault plane, critical slip displacement during stress

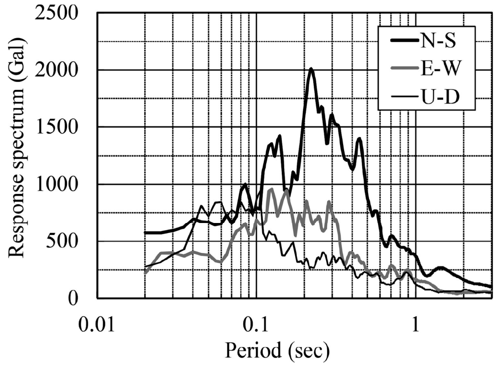

Figure 5. Acceleration response spectrum at K-NET Hakuba station.

Table 1. Geophysical parameters for numerical analysis.

Bedrock	
Elastic velocity of S wave, V_S (m/s)	3,500
Elastic velocity of P wave, V_P (m/s)	6,100
Unit weight, γ_t (kN/m^3)	26.5
Poisson's ratio, ν	0.25
Fault	
Shear stiffness, K_s (GN/m^3)	10, 1, 0.1, 0.01
Normal stiffness, K_n (GN/m^3)	$3\times K_s$
Static stress drop, $\Delta\tau_s$ (MPa)	2.0
Peak strength, τ_y (MPa)	15.2
Residual strength, τ_r (MPa)	10.0
Critical slip displacement, D_c (m)	0.0, 0.01, 0.05, 0.1, 0.2
Damping ratio, h	0.03
Division size FEM mesh of a fault plane, B (m)	500, 300, 200, 150

drop, we performed a series of fault rupture simulations under various conditions as given in Table 1. Young's modulus and Poisson's ratio are determined by P-wave and S-wave. The average static stress drop $\Delta\tau_s$ in the fault plane is calculated from seismic moment and fault area (Sato, 1989). The peak strength τ_y is determined based on knowledge that excess strength $\Delta\tau_e$ is 1.6 times of the static stress drop $\Delta\tau_s$ (Andrew, 1987) and the residual strength τ_r made 10.0 MPa larger enough than dynamic stress drop $\Delta\tau_d$. The shear stress at hypocenter is assumed to be slightly larger than the peak strength τ_y. The shear stress distribution on the fault plane is assumed to have a mountain shape and average static stress drop $\Delta\tau_s$ became 2.0 MPa (Tsuboi & Miura, 2000 and Fukushima et al., 2010).

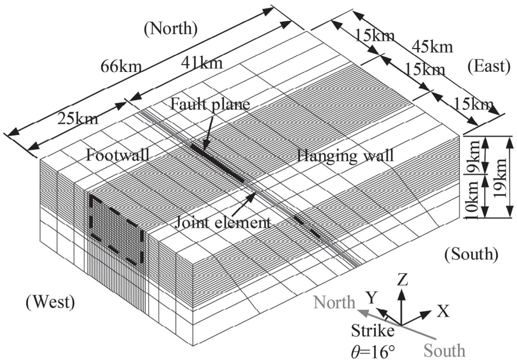

Figure 6. 3D-FEM model that the fault plane is divided into 500 m.

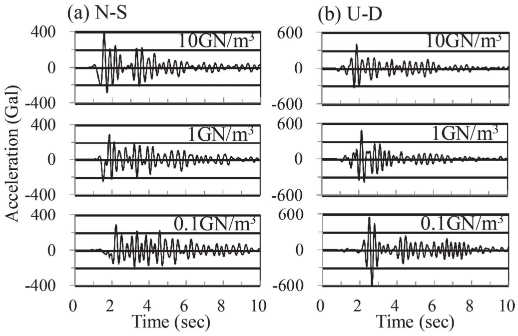

Figure 7. Comparison of analyzed acceleration waves at the ground surface in west 0.5 km from the surface rupture using different shear spring constants: $K_s = 10$, 1, 0.1 GN/m^3.

Figure 6 shows 3D-FEM model that the fault plane is divided into 500m. Joint elements are set up from north lateral boundary to south one and the strength of joint elements located in out of the fault plane is set to have larger value. The distance from the fault edge to the boundaries is more than fault length (15 km) and the viscous dampers are introduced at the lateral and bottom boundaries to absorb scattering wave energy. When a fault plane is divided at 150 m, the number of nodes becomes 175,032 and the number of elements is 163,212.

2000 steps with a time interval of 0.005 seconds was used for fault rupture simulation. Analyzed acceleration and displacement response are extracted at the ground surface in west 0.5 km from the surface rupture and compared with the observed surface ground motions recorded at K-NET Hakuba station to verify of parameters and modeling.

5 ANALYSIS RESULTS

5.1 *Influence of spring stiffness of joint element*

We carried out fault rupture simulations using different shear spring constants: K_s = 10, 1, 0.1, 0.01 GN/m3. Other parameters are set as follows: the damping ratio is 0.03, FEM mesh size of a fault plane is 500 m and critical slip displacement is zero.

Figure 7 compares analyzed acceleration waves at distances of 0.5 km west from the surface rupture. The amplitude of acceleration wave in N-S direction becomes smaller as shear spring constant decreases and it becomes larger in other directions. However, in the case of shear spring constant, that is, K_s = 0.01 GN/m3, the rupture does not propagate and the neighborhood of hypocenter is only ruptured. If a shear spring constant is set to have a smaller value, the shear stress of fault transferred from a yield element becomes smaller, and that of ground becomes larger. Therefore, the acceleration response in the fault plane direction, specifically, in N-S direction, becomes smaller, and the acceleration response in a direction perpendicular to fault plane, specifically, E-W and U-D direction, which greatly influence ground shaking, becomes larger.

Figure 8 shows the rupture propagation on the fault plane in the case of K_s = 1 GN/m3. As shown Figure 8(a), the rupture front spreads elliptically having the major axial direction along the slip direction and reaches the ground surface of fault center in 1.48 seconds. The rupture velocity from hypocenter to surface is 3.5 km/s. Generally the rupture velocity is around 0.8 times of *Vs* (Somerville *et al*, 1999). This calculated rupture velocity is slightly fast, however, when joint elements are used for a contact surface, spring constant should be large as much as possible. Therefore, K_s = 1 GN/m3 is used by the following calculation. Figure 8(b) shows the time histories of shear stress of the fault plane elements, which is shown in Figure 8(a): hypocenter, F-1 and F2. The shear stress is reduced to the residual strength just as shear stress reaches the peak stress. Accordingly the shear stress at hypocenter becomes equal to the residual strength. The shear stress increases in the element, which is near to the hypocenter, and reaches the failure limit. After reaching the peak stress level, the increase and decrease of shear stress occurs with yielding of neighboring elements.

5.2 *Influence of FEM mesh size of fault plane*

We performed fault rupture simulations using different FEM mesh size: B = 500, 300, 200, 150 m. Other parameters are set as follows: the damping ratio is 0.03, the spring stiffness of joint element is 1 GN/m3 and critical slip displacement is zero.

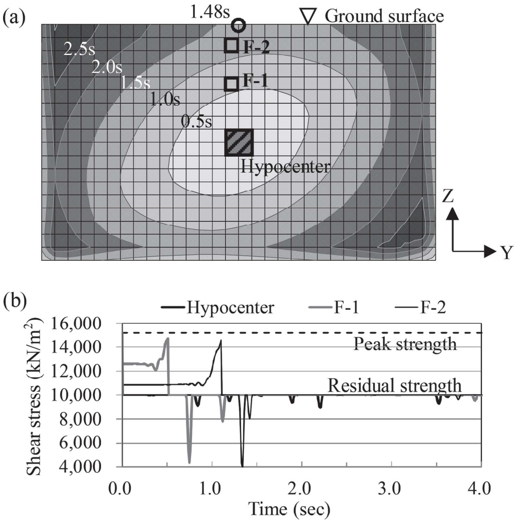

Figure 8. Rupture propagation on the fault plane in the case of $K_s = 1$ GN/m3: (a) Distributions of shear failure time, (b) Time histories of shear stress of the fault plane element.

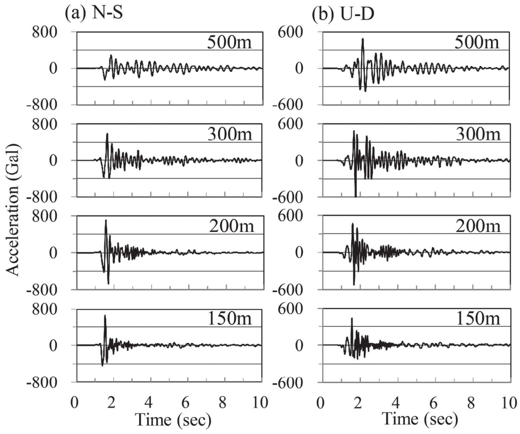

Figure 9. Comparison of analyzed acceleration waves at the ground surface in west 0.5 km from the surface rupture using different FEM mesh size: 500, 300, 200, 150 m.

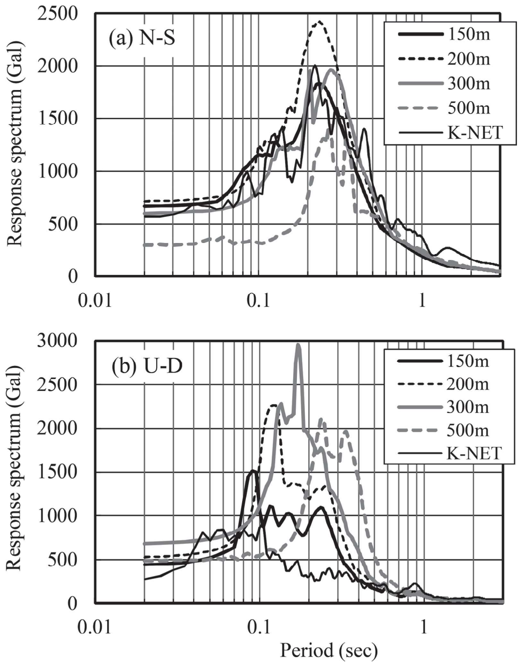

Figure 10. Comparison of acceleration response spectrum at the ground surface in west 0.5 km from the surface rupture using different FEM mesh size: 500, 300, 200, 150 m.

Figure 9 shows comparison of analyzed acceleration waves at distances of 0.5 km west from the surface rupture. When FEM mesh size becomes smaller, high frequency component of acceleration response increases and the response after main shock decreases because stress drop becomes small if FEM mesh size is small.

Figure 10 shows comparison between response spectra at distances of 0.5 km west from the surface rupture. Regarding the response spectra for E-W and U-D directions, the spectral peak shifts to the short period and becomes smaller as the FEM mesh size becomes smaller. As for response spectrum in N-S direction, the spectral peak slightly shifts to the short period and becomes larger. The response spectrum shape and peak value in N-S direction are closer to the observations if smaller mesh size is used. It is revealed that the response spectrum shape and peak value in horizontal direction can be simulated if mesh size is around 150 m, and it is also necessary to assume smaller mesh size to simulate the motions in vertical direction.

5.3 *Influence of critical slip distance in stress drop*

Fault rupture simulations were carried out using different critical slip displacement values: $D_c = 0.01, 0.05, 0.1, 0.2$ m. Other parameters are set as follows: the damping ratio is 0.03, the spring stiffness of joint element is 1 GN/m3 and FEM mesh size of a fault plane is 300 m.

Figure 11 shows a comparison of analyzed acceleration waves at distances of 0.5 km west from the surface rupture using different critical slip distance: $D_c = 0.01, 0.05, 0.1$ m. Furthermore, in the case of $D_c = 0.2$ m, the rupture does not propagate and only the neighbourhood of hypocenter is rup-

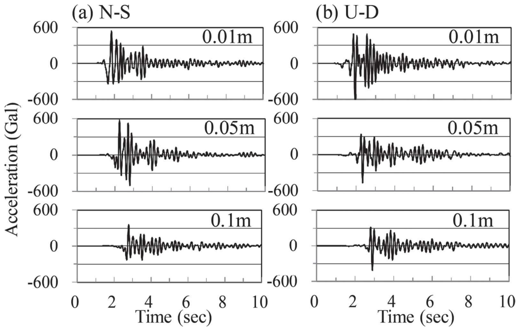

Figure 11. Comparison of analyzed acceleration waves at the ground surface in west 0.5 km from the surface rupture using different critical slip distance: D_c = 0.01, 0.05, 0.1 m.

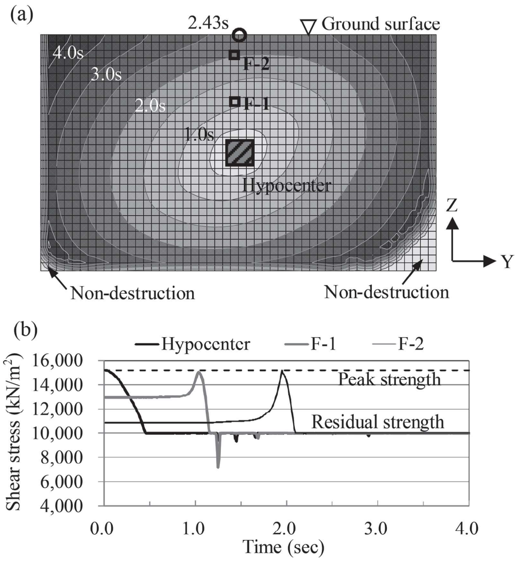

Figure 12. Rupture propagation on the fault plane in the case of D_c = 0.1 m: (a) Distributions of shear failure time, (b) Time histories of shear stress of the fault plane element.

tured. When critical slip distance becomes larger, the main shock is delayed and the amplitude of acceleration wave becomes smaller. The maximum acceleration occurs at around 2.8 seconds in case of D_c = 0.1 m. However, it is earlier than that of the observations.

Figure 12 shows the rupture propagation on the fault plane in the case of D_c = 0.1 m. Figure 12(a) shows the distributions of shear failure propagation time of the fault plane in the case of D_c = 0.10 m. The rupture front reaches the ground surface of fault center in 2.43 seconds and the lateral edges in 3.5–4.5 seconds. The rupture velocity from hypocenter to surface is 2.1 km/s. It is about 0.6 times of the elastic velocity of S wave and is slightly smaller

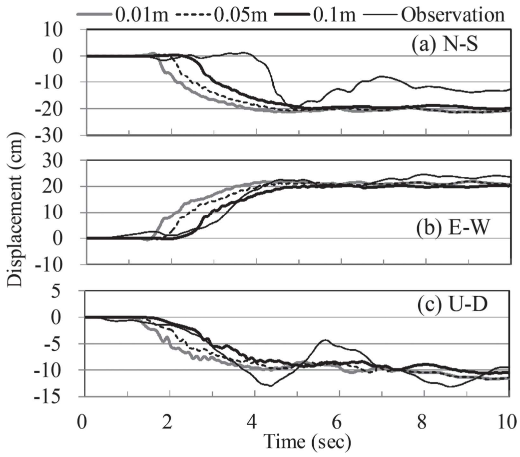

Figure 13. Comparison of analyzed displacement waves at the ground surface in west 0.5km from the surface rupture using different critical slip distance: D_c = 0.01, 0.05, 0.1 m.

than general rupture velocity. When critical slip distance is not considered, yielding spreads over the whole fault plane. To stop yielding, the strength of joint elements located in out of fault plane is set large value. However, no failure area remains in the bottom end of right and left when critical slip distance is considered. It implies that the spread of rupture could be stopped even if the ruptured area of fault plane was not set previously using appropriate quantity of critical slip distance and stress drop. Figure 12(b) shows the time histories of shear stress of the fault plane element in the case of D_c = 0.10 m. Relation between slip distance and stress drop is linear as seen in Figure 2, although time variation of shear stress during stress drop is convex. It indicates that sliding of fault increases moderately.

Figure 13 compares analyzed displacement response during rupturing. Similarly, the displacement is delayed as the slip distance becomes larger. However, the permanent displacement for all cases is almost the same. The analyzed residual displacement is in good agreement with the actual displacement.

6 CONCLUSIONS

In this study, we performed a series of fault rupture simulations using 3D-FEM for the 2014 Northern Nagano Earthquake and evaluated the influences of FEM mesh and various conditions. The findings obtained from this study can be summarized as follows:

1. The horizontal acceleration is well simulated if a fault plane is discretized into small FEM mesh

less than 150 m. However, it is also necessary to discretize vertical direction into smaller finite elements in order to evaluate the vertical component of ground acceleration.
2. The peak acceleration and displacement are delayed as the shear spring constant becomes smaller and/or critical slip displacement becomes larger.
3. When the spring constant is less than 0.01 GN/m3 or critical slip displacement is more than 0.2 m, the rupture does not propagate and only the neighborhood of hypocenter is ruptured.
4. It is possible to simulate displacement and strong motion simultaneously using appropriate parameters and discretizing a fault plane into small FEM mesh less than 150 m.

We continue to simulate other earthquakes and examine the validity and the applicability of numerical method and modeling of a fault presented in this study.

REFERENCES

Andrews, D.J. 1976. Rupture velocity of plane strain shear racks. *J. of Geo. Res.* 81(32): 5679–5687.

Aydan, O. & Ohta, Y. 2011. The erratic pattern screening (EPS) method for estimation of co-seismic deformation of ground from acceleration records and its application. *Seventh National Conf. on Earth. Eng.*, Turkey.

ERI (Earthquake Research Institute, University of Tokyo). 2014. Report of North Nagano Earthquake on November 22, 2014 (in Japanese).

F-net (Full Range Seismograph Network of Japan). 2014. Topics: Earthquake in North Nagano on November 22, 2014 (in Japanese).

Fukushima, K., Kanaori, Y. & Miura, F. 2010. Influence of fault process zone on ground shaking of inland earthquakes: verification of Mj = 7.3 Western Tottori Prefecture and Mj = 7.0 West Off Fukuoka Prefecture earthquakes, southwest Japan, *Eng. Geo.* 116: 157–165.

Iwata, N., Adachi, K., Takahashi, Y., Aydan, Ö., Tokashiki, N. & Miura, F. 2016. Fault rupture simulation of the 2014 Kamishiro Fault Nagano Prefecture Earthquake using 2D and 3D-FEM. *Proc., EUROCK 2016, Turkey*: 803–808.

JMA (Japan Meteorological Agency). 2014. News release document about the earthquake of North Nagano on November 22, 2014 about 22:08 (in Japanese).

Ohnaka, M. & Yamashita, T. 1989. A cohesive zone model for dynamic shear faulting based on experimentally inferred constitutive relation and strong motion source parameters. *J. Geophys. Res.* 94: 4089–4104.

Sato, R. 1989. Japanese seismic dislocation parameter handbook, *Kashima publication society* 309 (in Japanese).

Somerville, P.G., Irikura, K., Graves, R., Sawada, S., Wald, D., Abrahamson, N., Iwasaki, Y., Kagawa, T., Smith, N. & Kowada, A. 1999. Characterizing crustal earthquake slip models for the prediction of strong ground motion. *Seismological Research Letters* 70: 59–80.

Toki, K. & Miura, F. 1985. Simulation of a fault rupture mechanism by a two-dimensional finite element method. *J. Phys. Earth.* 33: 485–511.

Toki, K. & Sawada, S. 1988. Simulation of the fault rupture process and near filed ground motion by the three-dimensional finite element method. *Proc. of 9th World Conf. on Earth. Eng., Japan* II: 751–756.

Tsuboi, T. & Miura, F. 2000. Simulation of Near field Seismic Ground motions by FEM Considering Source Rupture Mechanism. *Proc. of the 12th World Conference on Earth. Eng.* (CD-ROM), Paper 271/4/A.